The magnetopause deformation indicated by fast cold ion motion

Wenlong Guo[1], Binbin Tang[2], Qinghe Zhang[1], Wenya Li[2], Zhongwei Yang[2], Tianran Sun[2], Jiuqi Ma[3], Xiaoxin Zhang[4], Xiaocheng Guo[2], and Chi Wang[2]

[1]Shandong Provincial Key Laboratory of Optical Astronomy and Solar-Terrestrial Environment, Institute of Space Sciences, Shandong University, Weihai, China.
[2]State Key Laboratory of Space Weather, National Space Science Center, Chinese Academy of Sciences, Beijing, China.
[3]School of Earth and Space Sciences, University of Science and Technology of China, Hefei, China.
[4]Key Laboratory of Space Weather, National Center for SpaceWeather, China Meteorological Administration, Beijing, China.

Key Points:

- The magnetopause is found to be significantly deformed with the presence of fast-moving cold ions, whose speed can exceed $\sim$ 400 km s^{-1}.
- The inferred magnetopause deformation amplitude varies from $\sim$0.2 to 2.5 R_E.
- The observed magnetopause deformation prefers to occur under quasi-radial IMF and fast solar wind conditions.

Corresponding author: Binbin Tang and Qinghe Zhang, bbtang@spaceweather.ac.cn, zhangqinghe@sdu.edu.cn

Abstract

The magnetopause deformation due to the upstream magnetosheath pressure perturbations is important to understand the solar wind - magnetosphere coupling process, but how to identify such events from in-situ spacecraft observations is still challenging. In this study, we investigate magnetopause crossing events with fast-moving cold ions in the magnetosphere from Magnetospheric Multiscale (MMS) observations, and find when fast-moving cold ions are present at the magnetopause, they are closely associated with the magnetopause deformation, which is featured by fast magnetopause motion and significant magnetopause normal deflection from model predictions. Therefore, fast-moving cold ions can be a useful indicator to search for magnetopause deformation events. By integrating the cold ion speed, the inferred magnetopause deformation amplitude varies from 0.2 to $\sim$ 2.5 R_E. Further statistics indicate that such magnetopause deformation events prefer to occur under quasi-radial interplanetary magnetic field and fast solar wind conditions, suggesting high-speed magnetosheath jets could be one direct cause of magnetopause deformations.

1 Introduction

The magnetopause is a boundary that shields the Earth's magnetosphere from the shocked solar wind. Its size and configuration are acutely important when investigating interactions between the interplanetary and magnetospheric environments, as various processes, such as magnetic reconnection and surface waves, can occur at the magnetopause, enabling mass and energy transfer across it.

To a first-order approximation, the magnetopause can be effectively represented through empirical models on large scales. For example, its shape and location have been extensively functioned (e.g. Fairfield, 1971; Shue et al., 1997, 1998; Lin et al., 2010; Dmitriev et al., 2011; Liu et al., 2015; Nguyen et al., 2022), which helps researchers to gain a preliminary understanding of the magnetopause by providing a basic response of the magnetopause under different solar wind and magnetospheric conditions. The accuracy of some widely used empirical magnetopause models has been tested with a large database of in-situ spacecraft crossings (Staples et al., 2020). The result shows that the magnetopause model can be used to estimate magnetopause location to within $\pm$ 1 Earth radii (R_E) for the majority of magnetopause crossing events (74%), but sometimes discrepancies between measurements and model predictions can be large. This discrepancy can be partly attributed to the non-stationary nature of the magnetopause, which moves and changes under varying upstream plasma and magnetic field conditions. It is found that the usual magnetopause motion speed along its normal direction is around 40 km s^{-1} from in-situ spacecraft measurements (e.g. Phan & Paschmann, 1996; Paschmann et al., 2018), and the global simulations get a similar result (Xu et al., 2022). However, sometimes the magnetopause can move extremely fast, reaching to a speed over 200 km s^{-1} (Phan & Paschmann, 1996; Paschmann et al., 2018). Such fast magnetopause motion should be probably caused by rapid pressure variations in the upstream magnetosheath. Actually, the magnetosheath is highly turbulent (Karimabadi et al., 2014), and structures with transient pressure perturbations, such as mirror-mode waves, high-speed magnetosheath jets (HSJs), and downstream propagating solar wind/foreshock transients, can frequently occur. Impacts of these structures to the magnetopause can be hardly incorporated into empirical models due to their transient nature, but many related event studies have been performed.

Sibeck et al. (1999) has shown that the pressure within a hot flow anomaly (HFA, one typical solar wind transient structure) can be depressed by an order in magnitude with respect to the ambient background, allowing the magnetopause move outward about 5 R_E in 7 minutes during the impacting process. Such HFA impact to the magnetopause has been displayed in different events, which in general can lead into the fast magnetopause

compression and expansion (Sibeck et al., 2000; Jacobsen et al., 2009; Šafránková et al., 2012; Zhang et al., 2022). Similarly, HSJs with local pressure enhancements can induce obvious inward magnetopause motion, following by possible subsequent magnetopause rebound (Shue et al., 2009; Plaschke et al., 2018; X. Wang et al., 2023) and the observed magnetopause normal can significantly differ from model predictions (Escoubet et al., 2020). Accompanied with the magnetopause deformation, magnetic reconnection can be triggered at the magnetopause (Hietala et al., 2018; Ng et al., 2021), waves can be generated in the magnetosphere (Katsavrias et al., 2021), and the ionosphere can have some response as well (B. Wang et al., 2018). Therefore, investigations of the magnetopause deformation caused by these pressure perturbation structures are very helpful to understand the solar wind-magnetosphere coupling process, as their occurrence rates are not rare (Plaschke et al., 2016; Schwartz et al., 2000). However, due to limited cross-sections of these structures (for example, the spatial scale of HSJs varies from $\sim$0.1 to $>$1 R_E (Plaschke et al., 2016, 2020)), the investigation of their impact to the magnetopause is still insufficient, which can be attributed to the difficulty in tracing the magnetopause response from in-situ spacecraft measurements.

Cold ions of ionospheric origin are often present in the magnetosphere (André & Cully, 2012). Due to the frozen-in nature of cold ions, they usually convect with magnetic field lines in the direction perpendicular to the magnetic field and they can be detected by on board particle instruments when cold ions get a relatively large bulk energy to overcome the spacecraft potential. Frequently, cold ions can reach to the magnetopause, and evolve into processes at the magnetopause, such as magnetic reconnection (Toledo-Redondo et al., 2016, 2021; Li et al., 2017). The cold ion speed at the magnetopause is often tens of km s^{-1}. In this study, we show that the speed of cold ions can reach to several hundreds of km s^{-1}, which can be taken as a good indicator for magnetopause deformation, and the detection of fast-moving cold ions can be a useful tool to search for magnetopause deformation events.

2 Observation

In this study, we investigate magnetopause crossing events accompanied with fast-moving cold ions from MMS observations. We use magnetic field data from the fluxgate magnetometer (Russell et al., 2016), electric field data from the electric field double probes (Ergun et al., 2016; Lindqvist et al., 2016), and particle data from the fast plasma investigation (Pollock et al., 2016). Due to the small separation of four MMS spacecraft (typically only a few to tens of kilometers at the magnetopause), data from individual satellites appear almost identical, and we primarily present the data from MMS 1. Unless otherwise stated, all vectors are presented in geocentric solar magnetospheric (GSM) coordinates.

We select relevant magnetopause crossing events semi-manually using following criteria. First, the location where MMS cross the magnetopause is within a cone angle of 45° centered on the Sun-Earth line, allowing us to focus on events near the subsolar region. Second, the speed of cold ions is larger than 200 km s^{-1}, and V_x should be the major component. Third, sometimes cold ions are difficult to identify before reaching to the magnetopause, as they can be either heated or mixed with other ion populations in the magnetopause boundary layer. We limit the time difference between clear cold ion signatures and the magnetopause crossing is less than 10 seconds, ensuring that the cold ion motion can be closely related to the magnetopause. Finally, the interplanetary magnetic field from OMNI should be stable at least for 15 min surrounding the magnetopause crossing, excluding the impact of the solar wind structures (such as magnetic discontinuities) to the magnetopause. If there are data gaps in the OMNI data set, we use time-shifted ACE data instead.

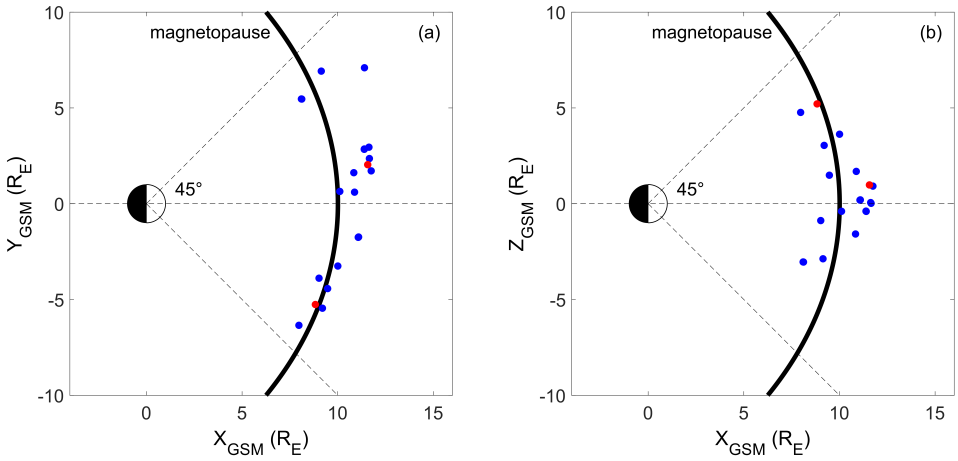

Figure 1. Locations of selected magnetopause crossings with fast cold ion motion as observed by MMS, which have been projected into the (a) X-Y and (b) X-Z planes in geocentric solar magnetospheric coordinates. The solid black lines represent the magnetopause, and the red dots show the location of two events detailed presented in Figure 2 and Figure 3.

Figure 1 shows locations of thirty selected MMS magnetopause crossings from 2015 to 2021. These crossings are approximately evenly distributed in the dawn and dusk sides of the magnetopause, but have some north-south asymmetry as the apogee of MMS spacecraft precess northward in years. We also note that there is a seasonal bias in these events, as MMS dayside magnetopause crossings occur primarily during the winter seasons of the north hemisphere. This seasonal bias implies a bias in the dipole tilt angle. However, the dipole tilt angle could influence the cusp indentation more significantly, but has little effects on the shape of the dayside magnetopause according to empirical models (Shue et al., 1997; Lin et al., 2010). Therefore, this seasonal bias in this data set can be ignored.

In the following sections, we will first present two events as indicated by red dots in Figure 1 to show how fast cold ion motion is related to the magnetopause deformation, and then investigate the preferred solar wind conditions in a statistical view.

2.1 Event study

Figure 2 provides an overview of the magnetopause crossing from the magnetosheath to the magnetosphere on February 1, 2020. During this time interval, The MMS spacecraft are located approximately at (8.83 -5.26 5.21) R_E. The magnetopause is characterized by a large variation of the magnetic field ($\Delta B_Z > 50$ nT, Figure 2a), high asymmetry of plasma density (Figure 2c) and temperature (Figure 2e) and the appearance of high-energy ions at the magnetospheric side ($W_i > 10$ keV, Figure 2f). Meanwhile, there are some unusual features during this magnetopause crossing. Comparing to the plasma flows in the magnetosheath, which are diverted at the magnetopause with a speed less than 200 km s^{-1}, the plasmas just inside the magnetopause are not idle, which have a speed larger than the magnetosheath plasmas, primarily flowing sunward (Figure 2d). Correspondingly, the measured electric field is extremely large inside the magnetopause, reaching to $\sim$ 15 mV m^{-1} (Figure 2b). The related flow energy of the E×B drift speed is overplotted in Figure 2f, which varies with an cold ion population, except for some spin effect. This indicates that cold ions may be responsible for this large speed plasma motion. Figure 2n presents a 2D slice of ion velocity distributions in the $V_{E\times B} - V_B$ plane

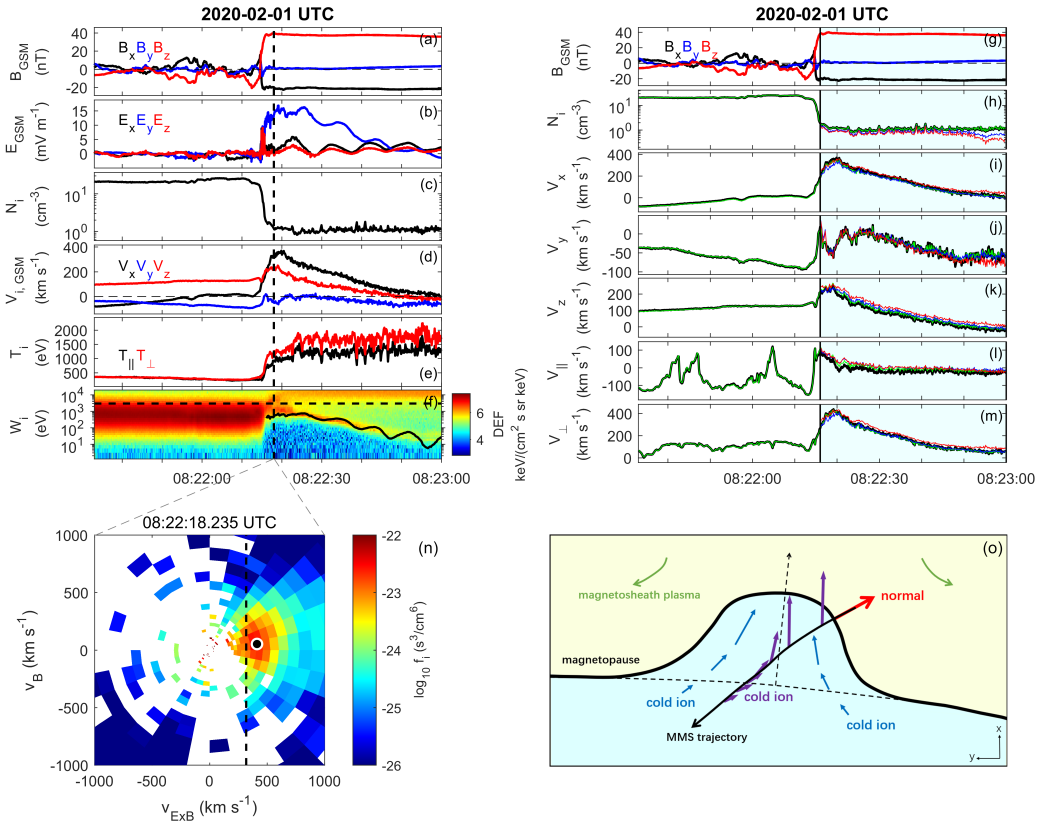

Figure 2. An overview of the magnetopause crossing on February 1, 2020. Panels at the left side show (a) magnetic field, (b) electric field, (c) ion number density, (d) ion velocity, (e) ion temperature, and (f) ion omnidirectional energy flux. Panels at the right side show (g) magnetic field, (h) the recalculated ion number density, and (i - m) the recalculated ion speed at different directions. The black curves represent the published data, and the green curves show the recalculated ion moments from velocity distributions. The partial cold ion moments are presented in blue and red curves, and the methods can be found in the context. (n) A two-dimensional slice of the ion velocity distribution at the time indicated by the vertical black line in panels (a - f). The dotted line in panel (n) indicates the electric drift speed, and the filled black dot shows the ion bulk speed. (o) A cartoon of the magnetopause deformation in this event. The magnetosheath and magnetosphere are displayed in yellow and cyan, and green and blue arrows indicate possible plasma flows in these two regions. The solid black arrow indicates the MMS trajectory during the magnetopause crossing and purple arrows show the observed cold ion velocities along MMS trajectory. The dotted black arrow and the red arrow are the predicted and observed magnetopause normal directions.

just inside the magnetopause (marked by the vertical dotted line in Figure 2a - 2f), in which we can find a relatively cold ion population that flows with a E×B speed (indicated by the dotted black line). This result is consistent with the frozen-in nature of cold ions, and magnetic flux tubes move with these cold ions at the magnetopause.

To further confirm these observations, we calculate the cold ion moments in different ways. First, we integrate the ion moments from measured velocity distributions (the green curves in Figure 2h - 2m), which are nearly identical with published data (the black curves). Then we separate the cold ion population, and calculate its partial moments dependently. The blue curves show the partial ion moments with energy lower than 3 keV (the horizontal line in Figure 2f), which exclude the high-energy magnetospheric ions, while the red ones present the results in a more careful way, which separates cold ions in the velocity phase space (Li et al., 2017). Though the calculated cold ion densities have some slight differences (Figure 2h), it clearly shows that cold ions are the major component inside the magnetopause. Therefore, the cold ion velocity is very similar to the velocity of all ions (Figure 2h - 2m). The maximum perpendicular speed of cold ions is $\sim$ 360 km s^{-1} when reaching to the magnetopause, and the parallel speed is relatively small. As cold ions are frozen-in with the magnetic field lines as shown above, the question now is how to understand these large sunward cold ion flows. For example, we should clarify these cold ions are flowing towards the magnetopause or moving with the magnetopause.

The magnetopause properties are investigated here. The four spacecraft timing method is applied to estimate the magnetopause normal direction and speed. It gives $V_{TM} \sim 156 \times$ [0.49 -0.83 0.26] km s^{-1} with estimated time delays from 08:22:14.20 to 08:22:16.00 UT. Using the same time interval, the magnetopause normal can be estimated based on the maximum variance analysis (MVA) on the magnetic field, yielding to N_{MVA} = [0.47 -0.81 0.34]. The difference of magnetopause normals from these two methods is about 6°, indicating reliability of the results. However, using the upstream solar wind parameters from OMNI data: N_{sw} = 3.9 cm^{-3}, V_{sw} = [457 11 -14] km s^{-1}, and B_{IMF} = [3.42 0.26 -0.17] nT, we can obtain the modeled magnetopause normal from the empirical magnetopause model (Shue et al., 1997), showing N_{SH} = [0.88 -0.33 0.33]. A large deflection of the magnetopause normal then can be found between the model and observations, reaching to 37°. This indicates that the magnetopause is at least locally deformed. Meanwhile, the magnetopause motion speed is much larger than its median value in statistics ($\sim$ 40 km s^{-1}, Paschmann et al., 2018), indicating fast outward motion of the magnetopause. If we project the cold ion speed at the time close to the magnetopause to the normal direction ($V_{cold,N}$, here we use the averaged normal flow speed from MVA and timing methods), $V_{cold,N}$ roughly matches the magnetopause motion speed ($\sim$ 156 km s^{-1}, Table 1), suggesting cold ions move with the magnetopause at a large speed. Figure 2o briefly summaries this event: the magnetopause is locally deformed, and MMS crosses the deformed magnetopause from one side, so that a large deflection of the magnetopause normal is observed. This also explains why there is a large cold ion speed tangential to the normal direction ($V_{cold,T}$, Table 1), as cold ions primarily flow sunward.

The cold ion speed decreases gradually when MMS goes into the magnetosphere, inferring MMS is moving away from the magnetopause. The distance between MMS spacecraft and the magnetopause is usually difficult to infer from in-situ measurements, but we can get its lower limit here by integrating the cold ion speed, showing that the magnetopause has moved about 1.3 R_E outward in 30 seconds. This result indicates that the magnetopause is significantly deformed in this event, and fast cold ions can be taken as a good indicator.

Figure 3 shows another magnetopause crossing event when MMS is located at [11.57 2.04 0.98] R_E on December 26, 2016. This event is in general similar to the first event, showing fast cold ion motion exceeding 400 km s^{-1} just inside the magnetopause, but this event also presents some different features. First, the sheath plasma flows have a

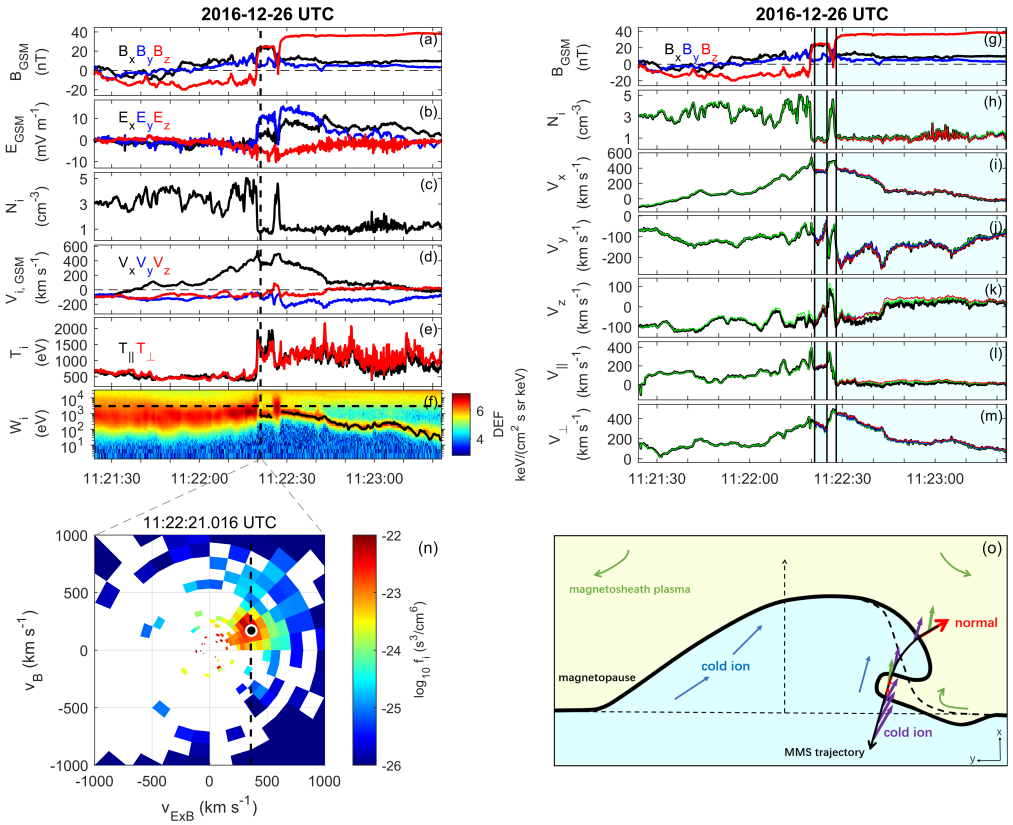

Figure 3. An overview of the magnetopause crossing on December 26, 2016. The figure format is similar to that in Figure 2.

Table 1. Magnetopause properties in Event 1 and 2.

Event	Time (UT)	Normal (Shue97)	V_{MP} (Timing, km s^{-1})	Normal (Timing)	Normal (MVA)	$V^{a}_{cold,N}$ (km s^{-1})	$V_{cold,T}$ (km s^{-1})	Deflection angle (°)
1	20200201/ 08:22:14.91	[0.88 -0.33 0.33]	156	[0.49 -0.83 0.26]	[0.47 -0.81 0.34]	213	290	37
2	20161226/ 11:22:19.55	[0.99 0.12 0.06]	276	[0.41 -0.86 -0.32]	[0.41 -0.89 -0.19]	280	218	73
	20161226/ 11:22:26.96		380	[-0.80 0.36 0.48]	[-0.80 0.35 0.49]	315	65	134
	20161226/ 11:22:27.14		474	[0.95 -0.18 -0.26]	[0.95 -0.21 -0.23]	444	101	27

[a] This $V_{cold,N}$ is the averaged value of the cold ion flow speed along the normal direction from the Timing and MVA method.

significant sunward component (Figure 3d). The speed of these sunward sheath plasma flows increases when getting closed to the magnetopause, reaching to 540 km s^{-1} just in front of the magnetopause. These anomalous sunward sheath plasma flows are the opposite of the usual anti-sunward magnetosheath flows, which are believed to be closely related with the magnetopause deformation as observed from THEMIS spacecraft (Shue et al., 2009), and the magnetopause is under the rebound motion. Second, MMS cross the magnetopause three times in 10 seconds. We check the magnetopause normal direction from these three magnetopause crossings from MMS, and find the magnetopause is largely deformed (Table 1). In particular, during the second magnetopause crossing from the magnetosphere to the sheath region, the sheath plasma keeps to move sunward, indicating the magnetopause still moves outward. If we define the magnetopause normal always pointing towards the magnetosheath, deflection of the observed magnetopause normal should be larger than 90° when comparing with empirical models (Figure 3o). This suggests that some secondary magnetopause distortion is formed, and its spatial scale is $\sim$ 100 km as the temporal separation of the last two magnetopause crossings is only about 0.2 s. By comparison, we can infer the magnetopause shift by integrating the cold ion motion, showing the magnetopause has at least moved outward for 2.5 R_E in 60 seconds.

2.2 Statistics

Two MMS magnetopause crossing events with fast cold ion motion have been presented, showing the magnetopause is not stationary and has been largely deformed at the same time. These observations suggest that fast-moving cold ions can be used as an indicator of the magnetopause deformation, based on two arguments. First, due to the frozen-in nature of cold ions, the magnetospheric magnetic flux should move with high-speed cold ions, which is associated with fast magnetopause motion. Second, the observed magnetopause normal is significantly deflected from the model predictions, indicating the magnetopause is locally deformed. This result is also supported by the clear cold ion flows tangential to the magnetopause (Table 1) and the gradual decrease of the cold ion speed as MMS goes into the magnetosphere (Figures 2 and 3). In this section, we will further examine these two arguments in a statistical view to investigate the relation between high-speed cold ions and the magnetopause deformation. To ensure the accuracy of statistical results, we have further applied an additional criterion (The angle of magnetopause normals from the Timing and MVA methods is less than 15°) when selecting the magnetopause crossing events. Figure 4a shows a scatter plot of the observed magnetopause speed versus the cold ion speed normal to the local magnetopause in all 30 magnetopause crossings, in which the positive/negative sign of the cold ion speed indicates the outward/inward magnetopause motion. A good linear relation between these two parameters with a slope close to 1 is revealed, showing fast cold ion motion is basically comparable to the high-speed magnetopause motion. Some events with inward

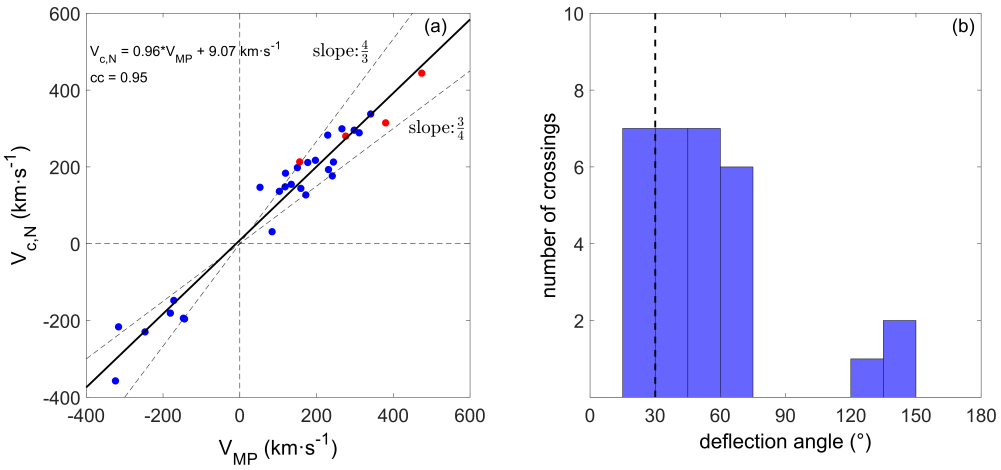

Figure 4. Statistics of the magnetopause crossings shown in Figure 1. (a) The scatter plot of the magnetopause' speed (V_{MP}) and the cold ion's speed along the normal direction($V_{c,N}$). The solid black line shows a linear fit of these two speeds. (b) Histogram of the deflection angles between the observed magnetopause normal and the prediction.

high-speed cold ions are also recorded, indicating the possible indentation of the magnetopause, but the event number is much fewer. Whether it suggests the earthward magnetopause motion is more difficult to reach a higher speed is not conclusive, as the event set used in this study is relatively small. The cold ion speed normal to the local magnetopause sometimes is lower than 200 km s^{-1} (the threshold set for previous event selection), and we attribute this to the local magnetopause deformation, which makes MMS cross the magnetopause from one side. Figure 4b then displays the histogram of deflection angles between MMS observations and model predictions. We find the deflection angle is usually larger than 30° in most magnetopause crossings, which is sufficiently larger than uncertainties of magnetopause normal directions (15°), and thus it indicates the magnetopause deformation is common when high-speed cold ions are present at the magnetopause. The deflection angles are larger than 90° in three cases, which are explained by secondary magnetopause structures as shown in Figure 3.

By integrating the cold ion speed along the MMS trajectory, we can estimate the amplitude of magnetopause deformation from in situ measurements as shown above. Here, if we combine successive magnetopause crossings (i.e. the three magnetopause crossings in the second case) into one event, 18 events are left from the total 30 magnetopause crossings. Figure 5 presents that the related magnetopause deformation amplitude of these events, which varies from 0.2 R_E to $\sim$ 2.5 R_E, and the meridian value is be approximately 1.2 R_E. We note that the magnetopause deformation amplitude calculated from the cold ion motion could be underestimated, but this result still indicates that the magnetopause is significantly deformed with the presence of high-speed cold ions. And fast-moving cold ions provide an applicable way to infer the magnetopause deformations.

Although we have shown fast-moving cold ions can be taken as an indicator of the magnetopause deformation, the observation of cold ions are locally at the magnetopause, meaning what causes the magnetopause deformation in the upstream solar wind is still unknown. Here, we check the occurrence of above 18 fast-moving cold ion events under different interplanetary magnetic field (IMF) cone angles (the angle between the IMF direction and the Sun-Earth line). Figure 6a shows that these events recorded prefer to occur under quasi-radial IMF conditions, and can be hardly found when IMF cone an-

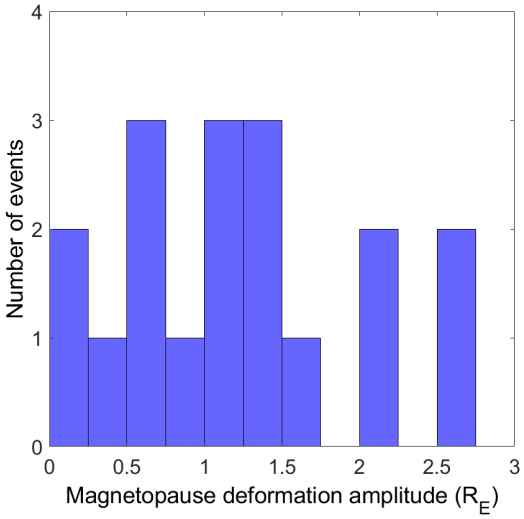

Figure 5. Statistics of magnetopause deformation amplitude of 18 magnetopause crossing events by integrating the cold ion speed.

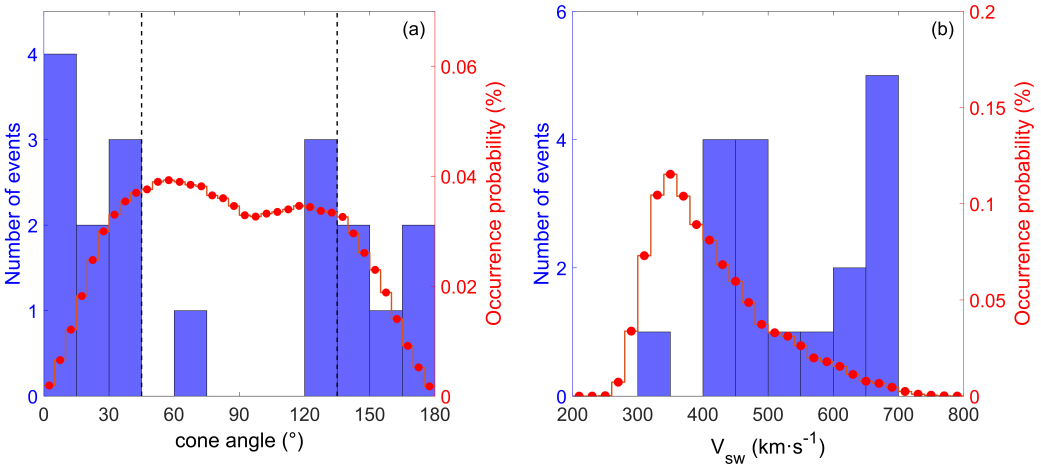

Figure 6. Statistics of related upstream solar wind conditions for the selected magnetopause crossing events. Panels show the number of events under (a) different IMF cone angles (the angle between the IMF direction and the Sun-Earth line) and (b) different solar wind speeds. The red lines show the occurrence probability of different IMF cone angles (a) and solar wind speeds (b) during MMS dayside magnetopause seasons from 2015 to 2021.

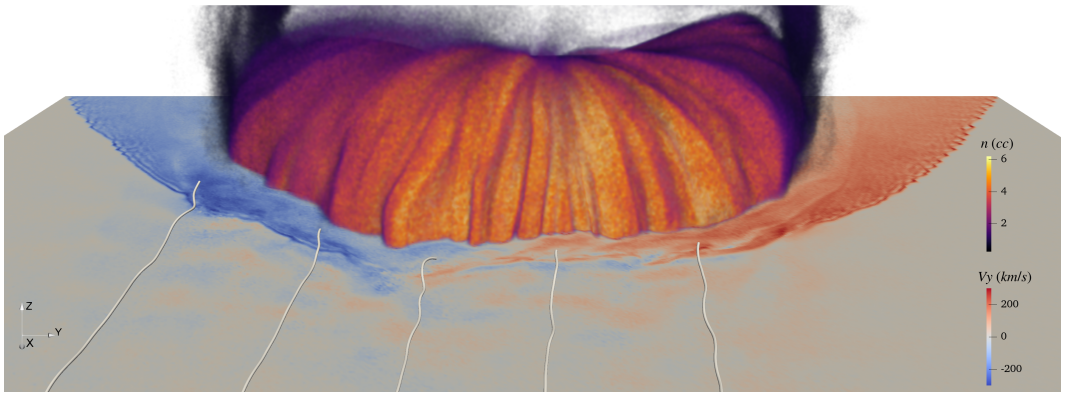

Figure 7. Magnetopause deformation from a 3-D global hybrid simulation under quasi-radial IMF condition. Several upstream IMF field lines are traced. The magnetopause location is estimated by the envelope of the 3-D density profile of ions trapped in the magnetosphere. A slice of solar wind ion bulk speed V_y is also plotted for reference.

gle is around 90°. To exclude the possible effect of the occurrence probability of the IMF cone angles, we calculate the IMF cone angle occurrence during MMS dayside magnetopause seasons from 2015 to 2021 (the red curve in Figure 6a). The result agrees well with Paker spirals, showing the peak occurrence is at cone angles around 45° and 135°. Therefore, 9 of 18 recorded events in Figure 6a that are found at cone angles $< 30°$ or $> 150°$ is not due to the uneven IMF cone angle effect, as the related occurrence probability of IMF cone angles is only 16.55 %. Similarly, these events tend to occur under higher solar wind conditions ($V_{sw} > 400$ km s^{-1}, Figure 6b). This tendency is also different with the solar wind speed distributions, which peaks at $V_{sw} \sim 350$ km s^{-1}.

As the fast-moving cold ions are locally observed by MMS at the magnetopause, their dependence on solar wind conditions is somewhat unexpected. Here we try to explore the possible relations between them. First, the quasi-parallel bow shock shifts to the nose region if the IMF cone angle is close to 0° or 180°, which would lead to a more turbulent environment extending to the upstream foreshock region and downstream magnetosheath. The high-speed magnetosheath jets with local dynamic pressure enhancement are then more frequently observed downstream of the quasi-parallel bow shock (Plaschke et al., 2018). These high-speed jets under fast solar wind conditions are more likely to pass through the magnetosheath and impact the magnetopause (LaMoury et al., 2021). As the typical size of a high-speed jet varies from 0.1 R_E to 1 R_E (Plaschke et al., 2016, 2020), the related magnetopause deformation is temporally and spatially limited, which results into fast magnetopause motion. Due to frozen-in nature of cold ions, they would therefore get a high speed, if they can appear at the magnetopause. Thus, this explains why fast-moving cold ions can be taken as an indicator of the magnetopause deformation. Figure 7 presents the local magnetopause deformation in a 3-D global hybrid simulation under quasi-radial IMF conditions (Yang et al., 2024), consistent with the process described above.

3 Summary

In this study, we have shown that cold ions at the magnetopause can sometimes reach to several hundreds of km s^{-1}, which are closely related to the magnetopause deformation from a statistical view. As the magnetopause deformation is not straightforward to be determined from in-situ measurements, this study suggests that fast-moving cold ions can be taken as a useful tool to identify the magnetopause deformation. In ad-

dition, we also found fast-moving cold ions at the magnetopause are favorable to occur when IMF is more flow-aligned and solar wind speed is higher. Therefore, we infer that high-speed magnetosheath jets could be one direct cause of the MMS observations locally at the magnetopause, as they are more frequently to occur under similar solar wind conditions. In other words, fast-moving cold ions are one direct consequence of the magnetopause impact of high-speed magnetosheath jets.

However, there are two things that should be further addressed. First, cold ions do not appear at the magnetopause all the time, and they are not evenly distributed along the magnetopause as well. So, although fast-moving cold ions can be taken as an indicator for the magnetopause deformation, not all magnetopause deformations are accompanied with cold ions. Due to the dawn-dusk asymmetry of cold ion appearance at the magnetopause, it is difficult to investigate if there are more magnetopause deformation events at dawn-side magnetopause, which is downstream of the quasi-parallel bow shock under the average Paker spirals. Second, the solar wind conditions are limited to be relatively stable in this study, which is of course good to reveal the relation between upstream solar winds and the local magnetopause processes. But the solar wind transient structures, such as HFAs, can also impact the magnetopause, leading to magnetopause perturbations. In fact, fast-moving cold ions have been observed in an extreme magnetopause motion event caused by an HFA (Jacobsen et al., 2009).

In general, fast-moving cold ions provide a new perspective to study the magnetopause response to the solar wind from in-situ measurements. The forthcoming Solar wind Magnetosphere Ionosphere Link Explorer (SMILE) mission aims to image the magnetopause with soft X-rays (C. Wang & Branduardi-Raymont, 2018; Branduardi-Raymont et al., 2018). If time series of magnetopause images are able to distinguish the local magnetopause deformation, some relevant joint studies can be performed between the global magnetopause images and the in-situ magnetopause crossings in the future.

Open Research Section

MMS data are available at the MMS Science Data Center (`https://lasp.colorado.edu/mms/sdc/public/about/browse-wrapper/`), and the solar wind data are accessible at the CDAweb (`https://cdaweb.gsfc.nasa.gov/pub/data/`). The IRFU-Matlab package (`https://github.com/irfu/irfu-matlab`) is used for data analysis. The magnetopause crossing list used in this study can be found at `https://zenodo.org/records/8283060`.

Acknowledgments

This work was supported by the National Key R&D Program of China (2021YFA0718600), the National Natural Science Foundation of China (grants 42188101, 42122032, 41974196, 42274211, and 41974170) and the Specialized Research Fund for State Key Laboratories of China.

References

André, M., & Cully, C. M. (2012). Low-energy ions: A previously hidden solar system particle population. *Geophysical Research Letters*, *39*(3).

Branduardi-Raymont, G., Wang, C., Escoubet, C. P., Adamovic, M., Agnolon, D., Berthomier, M., ... Zhu, Z. (2018). *SMILE definition study report* (V1.0 ed.; Tech. Rep.). ESA/SCI. doi: 10.5270/esa.smile.definition_study_report-2018-12

Dmitriev, A., Suvorova, A., & Chao, J.-K. (2011). A predictive model of geosynchronous magnetopause crossings. *Journal of Geophysical Research: Space Physics*, *116*(A5). doi: 10.1029/2010JA016208

Ergun, R., Tucker, S., Westfall, J., Goodrich, K., Malaspina, D., Summers, D., ...

others (2016). The axial double probe and fields signal processing for the MMS mission. *Space Science Reviews*, *199*(1-4), 167–188.

Escoubet, C. P., Hwang, K.-J., Toledo-Redondo, S., Turc, L., Haaland, S., Aunai, N., ... others (2020). Cluster and MMS simultaneous observations of magnetosheath high speed jets and their impact on the magnetopause. *Frontiers in Astronomy and Space Sciences*, 78.

Fairfield, D. H. (1971). Average and unusual locations of the Earth's magnetopause and bow shock. *Journal of Geophysical Research (1896-1977)*, *76*(28), 6700–6716. doi: 10.1029/JA076i028p06700

Hietala, H., Phan, T., Angelopoulos, V., Oieroset, M., Archer, M. O., Karlsson, T., & Plaschke, F. (2018). In situ observations of a magnetosheath high-speed jet triggering magnetopause reconnection. *Geophysical Research Letters*, *45*(4), 1732–1740.

Jacobsen, K., Phan, T., Eastwood, J., Sibeck, D., Moen, J., Angelopoulos, V., ... others (2009). Themis observations of extreme magnetopause motion caused by a hot flow anomaly. *Journal of Geophysical Research: Space Physics*, *114*(A8).

Karimabadi, H., Roytershteyn, V., Vu, H., Omelchenko, Y., Scudder, J., Daughton, W., ... others (2014). The link between shocks, turbulence, and magnetic reconnection in collisionless plasmas. *Physics of Plasmas*, *21*(6), 062308.

Katsavrias, C., Raptis, S., Daglis, I. A., Karlsson, T., Georgiou, M., & Balasis, G. (2021). On the generation of Pi2 pulsations due to plasma flow patterns around magnetosheath jets. *Geophysical Research Letters*, *48*(15), e2021GL093611.

LaMoury, A. T., Hietala, H., Plaschke, F., Vuorinen, L., & Eastwood, J. P. (2021). Solar wind control of magnetosheath jet formation and propagation to the magnetopause. *Journal of Geophysical Research: Space Physics*, *126*(9), e2021JA029592.

Li, W. Y., André, M., Khotyaintsev, Y. V., Vaivads, A., Fuselier, S., Graham, D. B., ... others (2017). Cold ionospheric ions in the magnetic reconnection outflow region. *Journal of Geophysical Research: Space Physics*, *122*(10), 10–194.

Lin, R. L., Zhang, X. X., Liu, S. Q., Wang, Y. L., & Gong, J. C. (2010). A three-dimensional asymmetric magnetopause model. *Journal of Geophysical Research: Space Physics*, *115*(A4). doi: 10.1029/2009JA014235

Lindqvist, P.-A., Olsson, G., Torbert, R., King, B., Granoff, M., Rau, D., ... others (2016). The spin-plane double probe electric field instrument for MMS. *Space Science Reviews*, *199*(1-4), 137–165.

Liu, Z.-Q., Lu, J. Y., Wang, C., Kabin, K., Zhao, J. S., Wang, M., ... Zhao, M. X. (2015). A three-dimensional high mach number asymmetric magnetopause model from global MHD simulation. *Journal of Geophysical Research: Space Physics*, *120*(7), 5645–5666. doi: 10.1002/2014JA020961

Ng, J., Chen, L.-J., & Omelchenko, Y. (2021). Bursty magnetic reconnection at the earth's magnetopause triggered by high-speed jets. *Physics of Plasmas*, *28*(9).

Nguyen, G., Aunai, N., Michotte de Welle, B., Jeandet, A., Lavraud, B., & Fontaine, D. (2022). Massive multi-mission statistical study and analytical modeling of the Earth's magnetopause: 2. shape and location. *Journal of Geophysical Research: Space Physics*, *127*(1), e2021JA029774. doi: 10.1029/2021JA029774

Paschmann, G., Haaland, S., Phan, T., Sonnerup, B. Ö., Burch, J., Torbert, R., ... others (2018). Large-scale survey of the structure of the dayside magnetopause by MMS. *Journal of Geophysical Research: Space Physics*, *123*(3), 2018–2033.

Phan, T. D., & Paschmann, G. (1996). Low-latitude dayside magnetopause and boundary layer for high magnetic shear: 1. structure and motion. *Journal of Geophysical Research: Space Physics*, *101*(A4), 7801–7815.

Plaschke, F., Hietala, H., Angelopoulos, V., & Nakamura, R. (2016). Geoeffective jets impacting the magnetopause are very common. *Journal of Geophysical Re-*

search: Space Physics, *121*(4), 3240–3253.

Plaschke, F., Hietala, H., Archer, M., Blanco-Cano, X., Kajdič, P., Karlsson, T., ... others (2018). Jets downstream of collisionless shocks. *Space Science Reviews*, *214*, 1–77.

Plaschke, F., Hietala, H., & Vörös, Z. (2020). Scale sizes of magnetosheath jets. *Journal of Geophysical Research: Space Physics*, *125*(9), e2020JA027962.

Pollock, C., Moore, T., Jacques, A., Burch, J., Gliese, U., Saito, Y., ... others (2016). Fast plasma investigation for magnetospheric multiscale. *Space Science Reviews*, *199*(1-4), 331–406.

Russell, C., Anderson, B., Baumjohann, W., Bromund, K., Dearborn, D., Fischer, D., ... others (2016). The magnetospheric multiscale magnetometers. *Space Science Reviews*, *199*(1-4), 189–256.

Šafránková, J., Goncharov, O., Němeček, Z., Přech, L., & Sibeck, D. (2012). Asymmetric magnetosphere deformation driven by hot flow anomaly (ies). *Geophysical research letters*, *39*(15).

Schwartz, S. J., Paschmann, G., Sckopke, N., Bauer, T. M., Dunlop, M., Fazakerley, A. N., & Thomsen, M. F. (2000). Conditions for the formation of hot flow anomalies at Earth's bow shock. *Journal of Geophysical Research: Space Physics*, *105*(A6), 12639–12650.

Shue, J.-H., Chao, J., Fu, H., Russell, C., Song, P., Khurana, K., & Singer, H. (1997). A new functional form to study the solar wind control of the magnetopause size and shape. *Journal of Geophysical Research: Space Physics*, *102*(A5), 9497–9511.

Shue, J.-H., Chao, J.-K., Song, P., McFadden, J., Suvorova, A., Angelopoulos, V., ... Plaschke, F. (2009). Anomalous magnetosheath flows and distorted subsolar magnetopause for radial interplanetary magnetic fields. *Geophysical Research Letters*, *36*(18).

Shue, J.-H., Song, P., Russell, C., Steinberg, J., Chao, J., Zastenker, G., ... others (1998). Magnetopause location under extreme solar wind conditions. *Journal of Geophysical Research: Space Physics*, *103*(A8), 17691–17700.

Sibeck, D., Borodkova, N., Schwartz, S., Owen, C., Kessel, R., Kokubun, S., ... others (1999). Comprehensive study of the magnetospheric response to a hot flow anomaly. *Journal of Geophysical Research: Space Physics*, *104*(A3), 4577–4593.

Sibeck, D., Kudela, K., Lepping, R., Lin, R., Nemecek, Z., Nozdrachev, M., ... others (2000). Magnetopause motion driven by interplanetary magnetic field variations. *Journal of Geophysical Research: Space Physics*, *105*(A11), 25155–25169.

Staples, F., Rae, I., Smith, A., Raymer, K., Case, N., Rodger, C., ... others (2020). Do statistical models capture the dynamics of the magnetopause during sudden magnetospheric compressions? *Journal of Geophysical Research: Space Physics*, *125*(4), e2019JA027289.

Toledo-Redondo, S., André, M., Aunai, N., Chappell, C. R., Dargent, J., Fuselier, S., ... others (2021). Impacts of ionospheric ions on magnetic reconnection and earth's magnetosphere dynamics. *Reviews of Geophysics*, *59*(3), e2020RG000707.

Toledo-Redondo, S., André, M., Vaivads, A., Khotyaintsev, Y. V., Lavraud, B., Graham, D. B., ... Aunai, N. (2016). Cold ion heating at the dayside magnetopause during magnetic reconnection. *Geophysical Research Letters*, *43*(1), 58–66.

Wang, B., Nishimura, Y., Hietala, H., Lyons, L., Angelopoulos, V., Plaschke, F., ... Weatherwax, A. (2018). Impacts of magnetosheath high-speed jets on the magnetosphere and ionosphere measured by optical imaging and satellite observations. *Journal of Geophysical Research: Space Physics*, *123*(6), 4879–4894.

Wang, C., & Branduardi-Raymont, G. (2018). Progress of solar wind magnetosphere ionosphere link explorer(SMILE) mission. *Chinese Journal of Space Science*, *38*(5), 657–661.

Wang, X., Lu, J., Wang, M., Zhou, Y., & Hao, Y. (2023). Simultaneous observation of magnetopause expansion under radial imf and indention by hsj. *Geophysical Research Letters*, *50*(20), e2023GL105270.

Xu, Q., Tang, B., Sun, T., Li, W., Zhang, X., Wei, F., ... Wang, C. (2022). Modeling of the subsolar magnetopause motion under interplanetary magnetic field southward turning. *Space Weather*, *20*(12), e2022SW003250.

Yang, Z., Jarvinen, R., Guo, X., Sun, T., Koutroumpa, D., Parks, G., ... Wang, C. (2024). Deformations at Earth's dayside magnetopause during quasi-radial IMF conditions: Global kinetic simulations and soft X-ray imaging. *Earth and Planetary Physics*, *8*. doi: 10.26464/epp2023059

Zhang, H., Zong, Q., Connor, H., Delamere, P., Facskó, G., Han, D., ... others (2022). Dayside transient phenomena and their impact on the magnetosphere and ionosphere. *Space Science Reviews*, *218*(5), 40.